

# CrystEngComm

Accepted Manuscript



This is an *Accepted Manuscript*, which has been through the Royal Society of Chemistry peer review process and has been accepted for publication.

*Accepted Manuscripts* are published online shortly after acceptance, before technical editing, formatting and proof reading. Using this free service, authors can make their results available to the community, in citable form, before we publish the edited article. We will replace this *Accepted Manuscript* with the edited and formatted *Advance Article* as soon as it is available.

You can find more information about *Accepted Manuscripts* in the [Information for Authors](#).

Please note that technical editing may introduce minor changes to the text and/or graphics, which may alter content. The journal's standard [Terms & Conditions](#) and the [Ethical guidelines](#) still apply. In no event shall the Royal Society of Chemistry be held responsible for any errors or omissions in this *Accepted Manuscript* or any consequences arising from the use of any information it contains.

## ARTICLE

# Atomic structure of defects and interfaces in TiO<sub>2</sub>-B and Ca:TiO<sub>2</sub>-B (CaTi<sub>5</sub>O<sub>11</sub>) films grown on SrTiO<sub>3</sub>

Cite this: DOI: 10.1039/x0xx00000x

Received 00th January 2012,  
Accepted 00th January 2012

DOI: 10.1039/x0xx00000x

[www.rsc.org/](http://www.rsc.org/)Sung Joo Kim,<sup>a</sup> Kui Zhang,<sup>a</sup> Michael B. Katz,<sup>a</sup> Baihai Li,<sup>a</sup> George W. Graham,<sup>a</sup> and Xiaoqing Pan<sup>\*b</sup>

The bronze polymorph of titanium dioxide, TiO<sub>2</sub>-B, characterized by a crystal structure with relatively open layered geometry, is a material of interest for various energy applications, including photovoltaics, catalysts, and high-rate energy storage devices. The related phase, CaTi<sub>5</sub>O<sub>11</sub>, which serves as an effective template layer, when deposited on (100) SrTiO<sub>3</sub>, for the growth of high quality single crystalline films of TiO<sub>2</sub>-B, is also of interest for such applications. In both materials, a detailed understanding of film growth and defect structure is deemed critical to the successful realization of these applications in thin film devices. Thus, using results obtained with aberration-corrected transmission electron microscopy, we present an analysis of defect and interfacial structure in CaTi<sub>5</sub>O<sub>11</sub> films grown on (100) and (110) SrTiO<sub>3</sub> substrates, as well as in the TiO<sub>2</sub>-B film grown on (001) CaTi<sub>5</sub>O<sub>11</sub>.

## 1. Introduction

Metal oxide thin films have attracted massive research interest, since intriguing chemistry from electron-electron interaction gives rise to unique properties that determine material functionality. Specifically, transition metal oxides with strongly correlated d-orbital electrons are under active scrutiny for piezoelectric<sup>1</sup>, photovoltaic<sup>2</sup>, and electrochemical applications<sup>3</sup>. Recently, there has been tremendous interest in the bronze polymorph of TiO<sub>2</sub> (here designated TiO<sub>2</sub>-B) due to its intriguing structure, which is composed of edge- and corner-sharing TiO<sub>6</sub> octahedra.<sup>4-6</sup> Compared to other polymorphs, such as anatase and rutile, bronze has the lowest density due to large, open channels suitable for diffusion of ionic species. This unique characteristic has triggered extensive study of various properties of TiO<sub>2</sub>-B including electronic, vibrational properties<sup>7</sup>, structural stability<sup>8</sup>, water adsorption<sup>9</sup>, and lithium ion transport<sup>4-5,10-13</sup>. Films of TiO<sub>2</sub>-B have many possible applications, including dye-sensitized solar cells (DSSCs)<sup>14-15</sup> and Li ion batteries. TiO<sub>2</sub>-B can potentially be used as a dye-absorbent for DSSCs because of its exceptional surface reactivity, comparable to that of commonly used anatase (here designated TiO<sub>2</sub>-A)<sup>16-17</sup>. It has been reported that the (100) facet of TiO<sub>2</sub>-B is less surface stable but more reactive to a dye molecule than most facets of anatase. TiO<sub>2</sub>-B may also be used

as an anode material in Li ion batteries<sup>4-5,18-19</sup>. Open (001) plane channels in TiO<sub>2</sub>-B aligned parallel to [010] act as sub-surfaces for fast Li ion transport, hence, enhancing battery charging rate<sup>20</sup>.

Although crystallographic orientation plays a critical role in device functionality, it is difficult to control the growth of TiO<sub>2</sub>-B films due to lack of a lattice-matching substrate that can guarantee high crystallinity of the film. The use of a template layer has proven successful for single crystalline film growth of materials with low symmetry, especially when such a layer partially satisfies an epitaxial relationship with both film and substrate.<sup>21-22</sup> For a material of lower symmetry, like monoclinic TiO<sub>2</sub>-B, choices for the template layer are limited by availability of crystal types similar to that of TiO<sub>2</sub>-B that also have a small lattice mismatch with a substrate. We have identified such a template layer, however, and have succeeded in growing it on SrTiO<sub>3</sub> (STO) substrates using pulsed-laser deposition (PLD).<sup>13,23</sup> The template phase, a Ca modification to the TiO<sub>2</sub>-B structure (here referred to as Ca:TiO<sub>2</sub>-B) with the formula CaTi<sub>5</sub>O<sub>11</sub>, is composed of a Ca bonded TiO<sub>x</sub> layer intercalated in between left c-oriented and right c-oriented TiO<sub>2</sub>-B layers.<sup>13</sup> By using high-resolution transmission electron microscopy (HRTEM), we have examined both the c-axis growth and off-c-axis growth (tilted 45° to the substrate

normal) of Ca:TiO<sub>2</sub>-B, respectively, on (100) and (110) STO substrates. Interestingly, we have found that these films may also serve as an anode material for a Li ion battery that exhibits high capacity and significantly enhanced rate capability.<sup>13</sup> More to the point, (001) Ca:TiO<sub>2</sub>-B provides a suitable template layer for c-axis growth of high quality TiO<sub>2</sub>-B films.

In addition to its value for optimizing film growth of the Ca:TiO<sub>2</sub>-B phase (and the TiO<sub>2</sub>-B phase deposited on top) along different orientations, the careful study of interfacial structures and various types of defects within the film is important since defects can potentially influence device characteristics. Hence, in the present work, using aberration-corrected scanning transmission electron microscopy (STEM), we perform a detailed study of three sets of films and discuss two main aspects: 1) interfacial structure and defects associated with the growth of Ca:TiO<sub>2</sub>-B films on (100) and (110) STO substrates, and 2) defect structure associated with subsequent growth of a (001) TiO<sub>2</sub>-B film on (001) Ca:TiO<sub>2</sub>-B.

## 2. Experimental

### 2.1 Synthesis of Ca:TiO<sub>2</sub>-B (CaTi<sub>5</sub>O<sub>11</sub>) and TiO<sub>2</sub>-B thin films

The CaTi<sub>4</sub>O<sub>9</sub> target used to grow Ca:TiO<sub>2</sub>-B thin films was fabricated by mixing 80 % TiO<sub>2</sub> and 20 % CaO powders, sintering at 1400 °C, and pressing a pellet under force equivalent to 10,000 lb (or 4535 kg). The TiO<sub>2</sub> target used to grow TiO<sub>2</sub>-B thin films was made from pure TiO<sub>2</sub> powder in like manner. The vacuum chamber for PLD has a base pressure of <10<sup>-7</sup> Torr. A 248 nm KrF excimer laser with a pulse duration of 22 ns and a fluence of ~3.4 Jcm<sup>-2</sup> was used for the film deposition at a repetition rate of 10 Hz. The target-to-substrate distance was set to 6.35 cm. All thin film deposition was done at 800 °C in an oxygen ambient of 0.05 Torr with a deposition rate of 0.01-0.02 Å/pulse. The deposited film thickness was in the range of 5-200 nm, which was measured by a Veeco Dektak profilometer and confirmed with TEM. Additional details regarding the PLD growth of these films may be found in Ref. 23.

### 2.2 Structural characterization of thin films

All high-angle annular dark field (HAADF) images were taken using a spherical aberration-corrected STEM (JEM JEOL-2100F), operated at 200 kV. Cross-sectional TEM specimens were prepared via mechanical polishing and ion-milling under Ar gas at 4 kV.

## 3. Results

### 3.1 Overview of films grown on (100) and (110) STO substrates

Films of Ca:TiO<sub>2</sub>-B were deposited by PLD on both (100) and (110) STO substrates at 800 °C using a PLD target composed of CaTi<sub>4</sub>O<sub>9</sub>. A film of the regular TiO<sub>2</sub>-B was subsequently deposited by PLD on the Ca:TiO<sub>2</sub>-B film on the (100) STO substrate at 800 °C using a PLD target composed of pure TiO<sub>2</sub>.

As shown schematically in Fig. 1a and 1b, growth of Ca:TiO<sub>2</sub>-B is highly dependent on the STO orientation. Whereas growth on (100) yields a smooth, epitaxial film that provides a good template for subsequent growth of TiO<sub>2</sub>-B (Fig. s1, see Supporting Information), growth on (110) initially results in a mixture of CaTiO<sub>3</sub> (here designated as CTO) and TiO<sub>2</sub>-B at the interface, yielding a film with many more defects and a rough surface that does not support the subsequent growth of a high quality TiO<sub>2</sub>-B film. These features are illustrated by the STEM images shown in Fig. 1c and 1d. Detailed differences and thorough analyses of interface and film structures are discussed below.

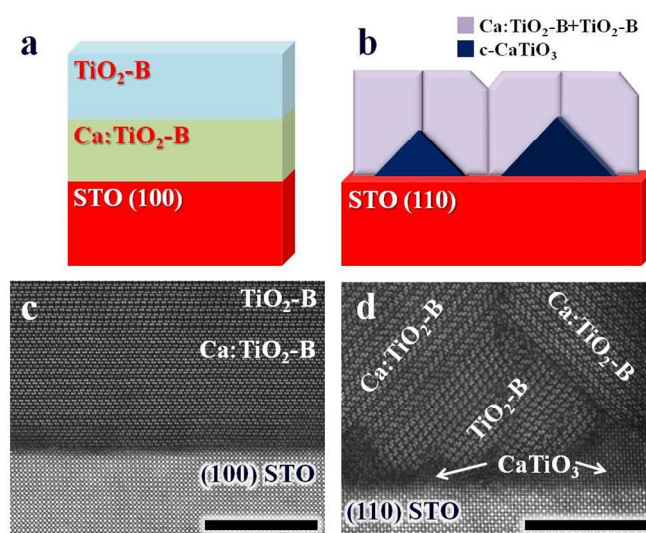
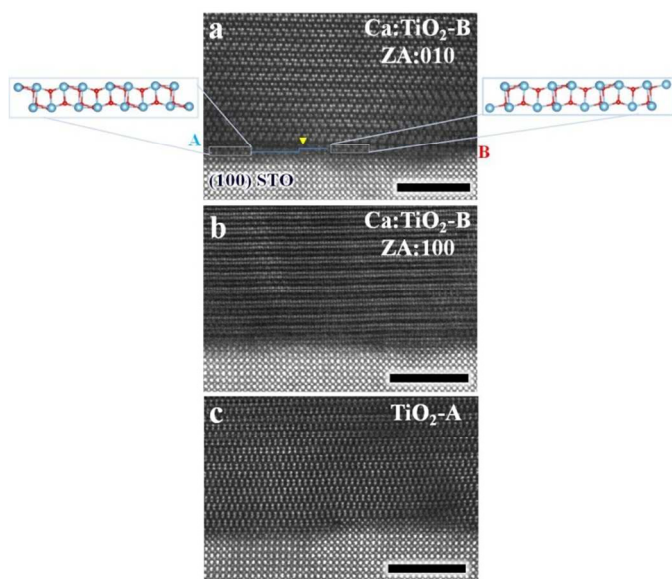


Fig. 1 Schematics and corresponding high-resolution STEM images of films grown on (a,c) (100) and (b,d) (110) STO substrates. Scale bars are 10 nm.

### 3.2 Interfacial structure and defects in a Ca:TiO<sub>2</sub>-B film grown on (100) STO

For the c-axis growth of a Ca:TiO<sub>2</sub>-B film, the titania polymorph that prefers to grow, TiO<sub>2</sub>-A, competes with Ca:TiO<sub>2</sub>-B to form an epitaxial interface with (100) STO. For Ca:TiO<sub>2</sub>-B, since both in-plane *a* and *b* cell parameters are almost integer multiples of the lattice parameter of STO, the film can have either a (100) plane or a (010) plane oriented parallel to the STO surface. TiO<sub>2</sub>-A, despite similar lattice mismatch (~3 %), exhibits a better epitaxial relationship with STO because the square-shaped arrangement of Ti atoms within its c-plane provides a cube-on-cube relationship with the similarly configured TiO<sub>x</sub> termination of STO.<sup>24</sup> This characteristic naturally drives the growth of the TiO<sub>2</sub>-A on this substrate over a wide temperature range, 600-900 °C. Hence, along either the [100] or [010] direction, we observed the three differently configured interfaces between the film and STO: (100)Ca:TiO<sub>2</sub>-B||(100)STO, (010)Ca:TiO<sub>2</sub>-B||(100)STO, and (100)TiO<sub>2</sub>-A||(100)STO. Fig. 2 shows high-resolution STEM images of these three possible interfaces between the film and (100) STO. STO substrates in all three cases are atomically rough, in that there are several nm-wide steps with various

heights, also known as surface-step terraces (SSTs), which contribute to misfit strain with the epitaxial film.<sup>25-26</sup>



**Fig. 2** High-resolution STEM images of interfaces between STO and (a,b) Ca:TiO<sub>2</sub>-B and (c) TiO<sub>2</sub>-A resulting from growth of a Ca:TiO<sub>2</sub>-B film on (100) STO. A and B denote left and right c-orientation of a TiO<sub>x</sub> stack. Scale bars are 5 nm. Ti and O atoms are represented with blue and red, respectively.

Although this is expected to generate vertical mismatch gaps at opposite ends of the SSTs due to incomplete accommodation of full unit cell stacking (Fig. S2), the gaps were nevertheless filled by an additional vertical atomic plane during growth leading to local atomic rearrangement near the interface between the film and the substrate. This, in turn, would generate an elastic strain field near the interface, which affects the local atomic configuration of the Ca:TiO<sub>2</sub>-B (and TiO<sub>2</sub>-A) layer during continued growth. When comparing the three different interfaces, we observed that a Ca:TiO<sub>2</sub>-B layer does not accommodate SSTs of more than one-half unit cell high (Fig. 2a and 2b) whereas a TiO<sub>2</sub>-A layer accommodates SSTs as high as two unit cells, as shown in Fig. 2c. In addition to the cube-on-cube in-plane symmetry it shares with STO, TiO<sub>2</sub>-A also has good vertical matching with STO, corresponding to 4%. This is what enables TiO<sub>2</sub>-A to tolerate SSTs of any width and height. On the other hand, Ca:TiO<sub>2</sub>-B has a- and b-axis atomic configurations that are both different and have a larger vertical mismatch with STO. To tolerate even one-half unit cell surface roughness, as shown in Fig. 2a, Ca:TiO<sub>2</sub>-B needs to undergo local atomic ordering near the interface with STO. The first TiO<sub>x</sub> stack that is left c-oriented (here denoted as A) suddenly changes its stacking orientation to the right c-orientation (here denoted as B) along the same plane at the one-half unit cell SST (indicated with a line on either side of the arrow in Fig. 2a). This is due to the discontinuation of a Ca-modified TiO<sub>x</sub> layer at the SST in order to accommodate the vertical lattice mismatch generated by this step.

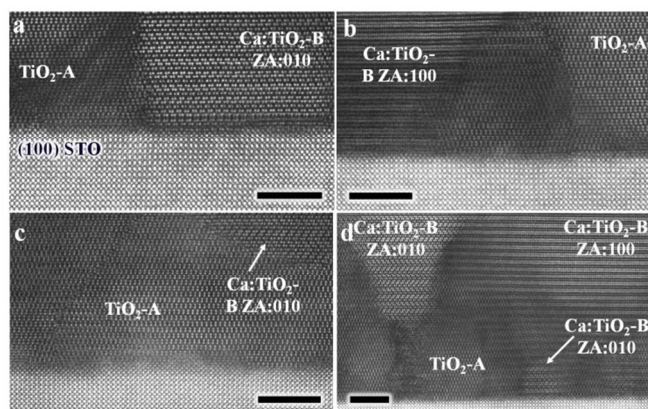


**Fig. 3** High-resolution STEM images of interphase boundaries between TiO<sub>2</sub>-A and Ca:TiO<sub>2</sub>-B along (a) [010] zone axis (ZA:010) and (b) [100] axis (ZA:100). (c,d) High-resolution STEM images of interphase boundaries formed via Ca:TiO<sub>2</sub>-B intergrowth from TiO<sub>2</sub>-A. Scale bars are 5 nm.

Another prominent defect in the Ca:TiO<sub>2</sub>-B film grown on (100) STO is the interphase boundary between Ca:TiO<sub>2</sub>-B and TiO<sub>2</sub>-A. Two of the major types of interface observed are (100)Ca:TiO<sub>2</sub>-B||{(100)TiO<sub>2</sub>-A (Fig. 3a) and (010)Ca:TiO<sub>2</sub>-B||{(100)TiO<sub>2</sub>-A (Fig. 3b). The first has a boundary complexion that is rough but relatively sharp compared to the second, which has smooth and diffuse boundary complexion because the (100) planar surface of Ca:TiO<sub>2</sub>-B is jagged due to repeated A- and B-orientation TiO<sub>x</sub> stacking. Hence, despite the similar lattice mismatch in the two boundaries, the different planar surface morphology induces differently shaped interphase boundaries. A third type of interphase boundary, (100)Ca:TiO<sub>2</sub>-B||{(010)Ca:TiO<sub>2</sub>-B (Fig. 3d), has a complexion much more diffuse than that of (010)Ca:TiO<sub>2</sub>-B||{(100)TiO<sub>2</sub>-A, with a width of 5-10 nm.

In addition to the vertical interphase boundaries, horizontal interphase boundaries were also observed in the Ca:TiO<sub>2</sub>-B film. These were formed when Ca:TiO<sub>2</sub>-B was deposited on top of an existing TiO<sub>2</sub>-A grain. For a non-flat TiO<sub>2</sub>-A base, two Ca:TiO<sub>2</sub>-B grains with two different in-plane matching relationships with (001) TiO<sub>2</sub>-A were observed. As illustrated in Fig. 3c and 3d, for (100)Ca:TiO<sub>2</sub>-B||{(100)TiO<sub>2</sub>-A, the boundary is sharp, as opposed to (010)Ca:TiO<sub>2</sub>-B||{(100)TiO<sub>2</sub>-A, where the boundary is diffuse over a wide extent along the c-axis. Other minor defects that were observed, such as tiny grains buried inside a much larger grain along the film interface with STO, similar to a Ca:TiO<sub>2</sub>-B grain buried inside a TiO<sub>2</sub>-A grain, are illustrated in Fig. 3d. These buried grains were identified in cross-sectional STEM as a lattice overlap between the small and larger grains of different phases.

### 3.3 Interfacial structure and defects in a Ca:TiO<sub>2</sub>-B film grown on (110) STO

Distinct from the direct epitaxial growth on (100) STO, the growth of Ca:TiO<sub>2</sub>-B films on (110) STO initially involves phase separation of Ca:TiO<sub>2</sub>-B into two different phases, TiO<sub>2</sub>-B and pseudo-cubic CTO before a continuous layer of Ca:TiO<sub>2</sub>-

B starts to grow. Hence, this growth is quite unique since the film templates itself with these secondary phases. Although there has been a number of studies on the separate growth of an ultra-thin template layer of a certain phase for the successive deposition of a film of the same phase<sup>27-28</sup>, there has not yet been any study on the naturally driven growth of a secondary phase, acting as a template for the growth of the main phase. As illustrated by the schematic (Fig. s3a) and STEM images (Fig. s3b and c), from each {100} facet of the triangular CTO islands on (110) STO, the growth of TiO<sub>2</sub>-B noticeably occurred along both in-plane and out-of-plane directions, forming grain boundaries with each other and interphase boundaries with neighboring naturally grown TiO<sub>2</sub>-A grains (Fig. s3b and s3c). The volume proportion of TiO<sub>2</sub>-A occupying the film grown on a (110) substrate is approximately 10-15 %, larger than that for the film grown on a (100) substrate (5-10 %).

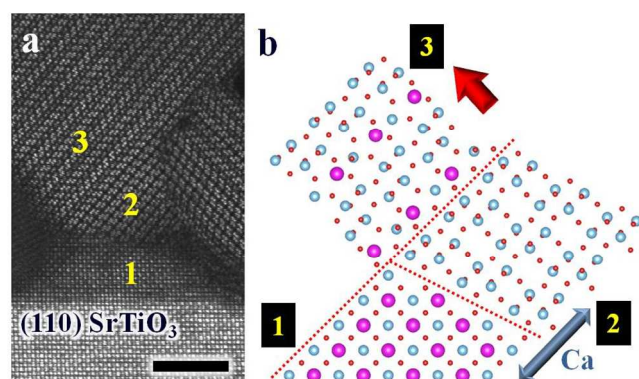


**Fig. 4** The growth of Ca:TiO<sub>2</sub>-B on (110) STO begins with Ca ion migration and formation of discrete layers of (1) CaTiO<sub>3</sub> and (2) TiO<sub>2</sub>-B which then acts as a template layer for deposition of (3) Ca:TiO<sub>2</sub>-b as shown in (a) high-resolution STEM images and (b) atomic model schematic: (1) CaTiO<sub>3</sub> and (2)TiO<sub>2</sub>-B are formed by phase separation via Ca flow. Scale bar is 5 nm.

The STEM image in Fig. 4a and schematic in Fig. 4b illustrate the possible steps involved in Ca:TiO<sub>2</sub>-B growth on (110) STO. The growth sequence of the layers on (110) STO may be: (1) CTO + (2) TiO<sub>2</sub>-B → (3) Ca:TiO<sub>2</sub>-B, which is different from that on (100) STO, where Ca:TiO<sub>2</sub>-B acts as a template layer for TiO<sub>2</sub>-B growth. Based on high-resolution images, it seems possible that phase separation occurred via some combination of Ca and Ti atom migration, allowing epitaxially more favorable formation of the CTO structure directly on (110) STO. Since (110) STO apparently does not support the direct growth of Ca:TiO<sub>2</sub>-B, which prefers to grow on (100), it is likely that (100) CTO induced the TiO<sub>2</sub>-B grains to form along its [100] direction (Fig. s4). Once a TiO<sub>2</sub>-B layer was well established, single-crystalline CaTiO<sub>2</sub>-B was able to grow along the c-axis of a TiO<sub>2</sub>-B template layer, essentially reversing the process that occurs on (100) STO.

As mentioned above, due to the nature of its growth, this film contains many grain boundaries between the two differently oriented Ca:TiO<sub>2</sub>-B grains and interphase boundaries formed between the tilted grains of TiO<sub>2</sub>-B, Ca:TiO<sub>2</sub>-B, and TiO<sub>2</sub>-A phases. This type of tilt boundary contains both ordered and

disordered complexions, marked with a rectangle and a circle, respectively in Fig. 5a. In the ordered region, a local, periodic atomic arrangement is present where (001) planes of alternating TiO<sub>x</sub> layers in a Ca:TiO<sub>2</sub>-B grain are coherently bonded to (100) planes of the adjacent TiO<sub>2</sub>-A grain. The red dots in Fig. 5a mark possible bonding sites for the Ti atoms from the two grains. While the ordered complexion is atomically sharp, the disordered complexion is rough, with random thickness; hence, the interphase boundary between Ca:TiO<sub>2</sub>-B and TiO<sub>2</sub>-A is also metastable. On the other hand, grain boundaries between Ca:TiO<sub>2</sub>-B grains, which are more commonly found throughout the film, do not exhibit any epitaxial relation between the grains, having simply been formed via 45° inter-penetration of adjacent grains growing towards each other along their a-axes (Fig. 5b).

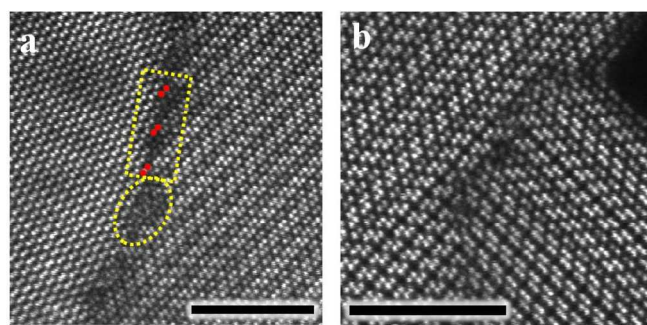


**Fig. 5** High-resolution STEM images showing (a) an interphase boundary between the Ca:TiO<sub>2</sub>-B and TiO<sub>2</sub>-A grains and (b) a grain boundary between the two abutting Ca:TiO<sub>2</sub>-B grains tilted 45° towards each other. A rectangle and a circle in (a) show locally ordered and disordered regions within the boundary. Scale bars are 5 nm.

Since the growth of TiO<sub>2</sub>-B films happened on facets of small CTO islands, the interfacial strain between their (100) planes is not significant enough to induce much misfit relaxation, even if the lattice mismatch (calculated for diagonal mismatch) between pseudo-cubic CTO and TiO<sub>2</sub>-B is close to 6 %. Nevertheless, a few of the larger sized TiO<sub>2</sub>-B grains possess several types of c-plane stacking defects. A good example is shown in Fig. 6a and represented schematically in Fig. 6e, where a few Ca-modified layers are intercalated within a TiO<sub>2</sub>-B grain, possibly due to incomplete phase separation between TiO<sub>2</sub>-B and CTO, making a layer of Ca:TiO<sub>2</sub>-B. In the same region, we also observed the sudden change in orientation of TiO<sub>x</sub> stacking (indicated with arrows in Fig. 6c). We speculate that this could indicate that there are missing c-planes of Ca-modified layers at those regions, and this could have resulted again from incomplete phase separation between TiO<sub>2</sub>-B and CTO. This possibility is reasonable since this defect feature, shown in a-direction growth of Ca:TiO<sub>2</sub>-B, is somewhat different from the case of c-growth of Ca:TiO<sub>2</sub>-B on (100) STO, where TiO<sub>x</sub> layer stacking is unidirectional unless a Ca-modified TiO<sub>x</sub> layer is present. However, despite these planar defects, since the growth of either a pure or an intermixed TiO<sub>2</sub>-B layer happened along the a-direction from CTO, any planar defects associated with this growth do not affect the Ca:TiO<sub>2</sub>-B

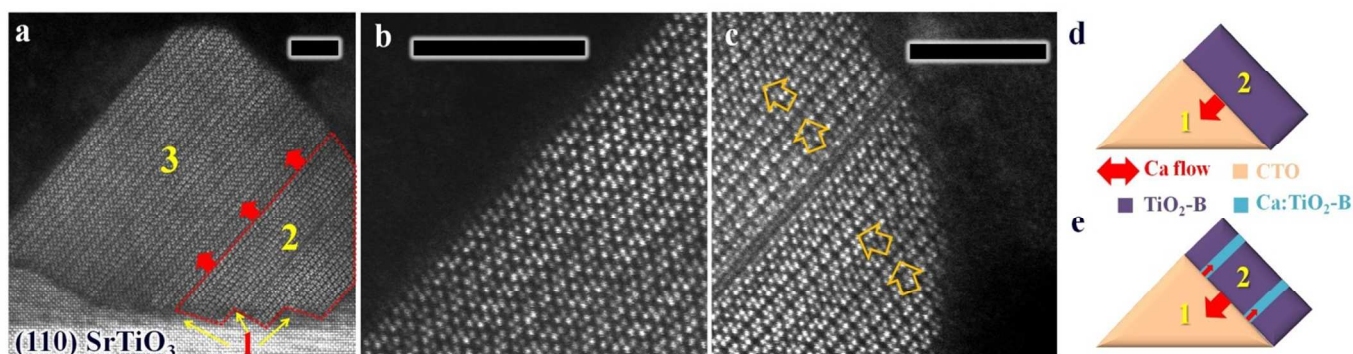


**Fig. 6** (a) An example of an intermixed 2: TiO<sub>2</sub>-B variant template layer due to intercalated calcium layers and its schematics (e). It is different from the perfect template layer as illustrated in Figure 5 and also as a schematics in (d) (b,c) High-resolution STEM images of layer 3 and 2, respectively. Scale bars are 5nm.

growth that happens from a c-plane of TiO<sub>2</sub>-B, so that defect-free single-crystalline grains could be grown, as shown in region 3 in **Figure 6b**.

### 3.4 Interfacial structure and defects in a TiO<sub>2</sub>-B film grown on (001) Ca:TiO<sub>2</sub>-B

Two main types of defects are present in a TiO<sub>2</sub>-B thin film grown on a (001) Ca:TiO<sub>2</sub>-B template, out-of-phase boundaries (OPBs) generated within a TiO<sub>2</sub>-B layer and interphase boundaries that are formed between TiO<sub>2</sub>-B and TiO<sub>2</sub>-A grains. OPBs are stacking defects induced by off-stoichiometry, or local deficiencies (e.g., missing rows of atoms) within a given layer or from an underlying layer. These are distinct from stacking faults that usually involve syntactic intergrowth of a differently configured layer of the same atomic type.<sup>29</sup> Using aberration-corrected atomic scale microscopy, we confirm that the local atomic misregistry within a Ca:TiO<sub>2</sub>-B template layer

is the origin of OPBs in the TiO<sub>2</sub>-B layer. As illustrated in Fig. 7 and 8, a locally missing Ca-modified TiO<sub>x</sub> layer in Ca:TiO<sub>2</sub>-B stacking ultimately generates a c-axis offset equivalent of 0.42c (where c is the c-axis lattice constant of TiO<sub>2</sub>-B) for a TiO<sub>2</sub>-B film deposited on top. In addition to a c-axis offset, local deficiency of Ca atoms also affects the orientation of a TiO<sub>2</sub>-B layer nucleated above, as shown schematically in Fig. 7c and 7d. This is due to the unique stacking sequence of Ca:TiO<sub>2</sub>-B that has a Ca-modified TiO<sub>x</sub> layer changing the orientation of a TiO<sub>x</sub>-only layer, for example, from A- to B-orientation and vice versa. Hence, the missing row of a Ca-modified TiO<sub>x</sub> in Ca:TiO<sub>2</sub>-B ultimately determines the orientation of two abutting TiO<sub>2</sub>-B layers with respect to the phase boundary during TiO<sub>2</sub>-B growth. When the deficiency happens at the surface of a Ca:TiO<sub>2</sub>-B layer, the resulting two abutting TiO<sub>2</sub>-B grains will face in and out from each other (Fig. 7a and 7b). However, when the missing Ca layer is in the middle of a CaTiO<sub>2</sub>-B layer, a single (Fig. 8a)

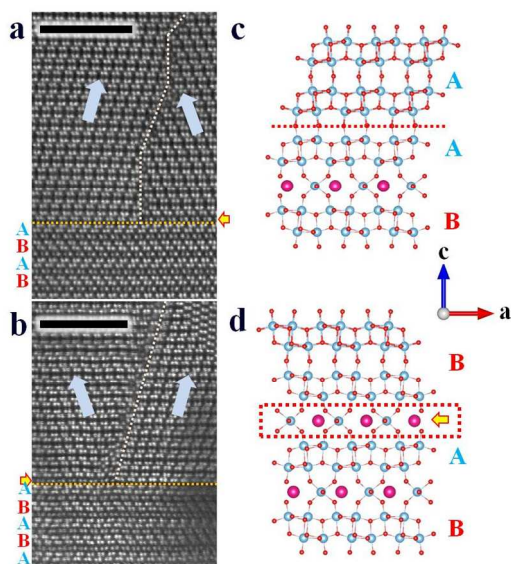


**Fig. 7** (a,b) High-resolution STEM images of defects at the interface between TiO<sub>2</sub>-B and Ca:TiO<sub>2</sub>-B that generate the two adjacent TiO<sub>2</sub>-B grains oriented opposite direction and (c,d) schematics of TiO<sub>2</sub>-B and Ca:TiO<sub>2</sub>-B interface without and with presence of Ca-modified layer indicated with the yellow arrow. Scale bars are 5nm.

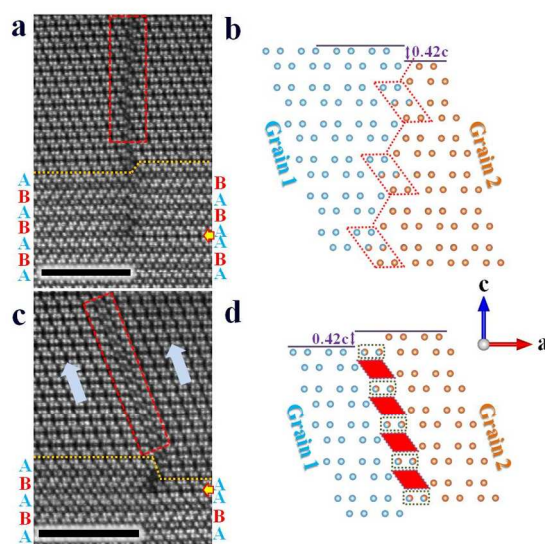


**Fig. 8** (a,c) High-resolution STEM images of defects at the interface between TiO<sub>2</sub>-B and Ca:TiO<sub>2</sub>-B with missing Ca-modified layer that generate the two adjacent TiO<sub>2</sub>-B grains oriented same direction. (b,d) Schematics of periodic boundary formed between the two adjacent grains from the regions marked with red in 3a and c. Sites with atoms marked with both gold and blue represent

possible occupancy sites for Ti atoms from either Grain 1 or Grain 2. Scale bars are 5nm.

or multi unit-cell surface step (Fig. 8c) is generated at the interface with a  $\text{TiO}_2\text{-B}$  layer and may result in  $\text{TiO}_2\text{-B}$  grains oriented in the same direction. Depending on the relative orientations of the two adjacent grains, the nature and orientation of OPBs can be different. When the two grains are oriented towards or away from each other, OPBs only have short-range or no periodicity (Fig. 7a and 7b). However, as in many cubic systems<sup>30-31</sup>, when the relative orientation of the two grains is along the same axis, OPBs have long-range crystallographic periodicity (Fig. 8). From the interface between  $\text{Ca}:\text{TiO}_2\text{-B}$  and  $\text{TiO}_2\text{-B}$ , a few mono-layers are needed for the boundary between the two  $\text{TiO}_2\text{-B}$  grains to become atomically ordered. Fig. 8 illustrates different examples of long-range atomic ordering achieved between two  $\text{TiO}_2\text{-B}$  grains oriented along the same direction. The periodic crystallographic patterns are presented with dotted lines. In both cases, there are possible sites for Ti atoms from the two abutting grains (here, labeled as Grain 1 and Grain 2 in the schematic representations in Fig. 8b and 8d) to share and form bonds. The atoms occupying these sites are presented with the two colors representative of Grain 1 and Grain 2. Even atoms that are displaced out from their original positions (Fig. 8c) that do not seem to belong to either of the two abutting grains (area marked with red in Fig. 8d) still have periodicity along the boundary. Another example is  $\text{Ca}:\text{TiO}_2\text{-B}$  grains having two missing Ca-modified layers near the interface between  $\text{TiO}_2\text{-B}$  and  $\text{Ca}:\text{TiO}_2\text{-B}$  with a multi unit-cell surface step (Fig. s5a). An OPB generated in between the two grains oriented in the same direction also has periodic crystallographic patterns again with possible sites for Ti atoms from either a left or right-side grain to occupy. (Fig. s5b)

The local misregistry of atomic stacking within a  $\text{Ca}:\text{TiO}_2\text{-B}$  layer can be attributed to the SSTs from the STO substrate, forming an interface with the  $\text{Ca}:\text{TiO}_2\text{-B}$  template layer. The interfacial strain between STO and  $\text{Ca}:\text{TiO}_2\text{-B}$  comes not only from the difference in their in-plane lattice parameters but also from the imperfect vertical matching between unit cells of the film and the termination surface of the substrate. Another possible way to understand the local misregistry in  $\text{Ca}:\text{TiO}_2\text{-B}$  is by considering growth characteristics of a thin film. The controlled growth of a thin film (e.g., via PLD) is highly unidirectional and performed under lower temperature conditions than bulk synthesis. Because lower temperature possibly hinders surface diffusion and structural rearrangement of Ca atoms, stacking defects are generated.

The second distinct defect in a  $\text{TiO}_2\text{-B}$  film is interphase boundaries between anatase and bronze polymorphs of  $\text{TiO}_2$  that were formed during growth. In conjunction with templated growth of  $\text{TiO}_2\text{-B}$ , some  $\text{TiO}_2\text{-A}$  grains grew simultaneously and formed a boundary with neighboring  $\text{TiO}_2\text{-B}$  and  $\text{Ca}:\text{TiO}_2\text{-B}$ , as shown in Fig. 9a and 9b. The boundary consists of disordered arrays and does not exhibit any epitaxial relationships; hence, complexions arising from this boundary

are most likely metastable. Looking into details, the interphase boundary between  $\text{TiO}_2\text{-A}$  and  $\text{TiO}_2\text{-B}$  grains is very sharp and uniform, with the width fluctuation from abutting phases varying only by a unit cell, whereas the boundary between  $\text{TiO}_2\text{-A}$  and  $\text{Ca}:\text{TiO}_2\text{-B}$  grains is relatively more diffuse over a wider thickness range. This qualitatively indicates that the boundary between  $\text{TiO}_2\text{-A}$  and  $\text{Ca}:\text{TiO}_2\text{-B}$  grains is more chemically unstable than between  $\text{TiO}_2\text{-A}$  and  $\text{TiO}_2\text{-B}$  grains. Aside from these large interphase boundaries, as described above, there are small sized micro-grains of  $\text{TiO}_2\text{-A}$  sandwiched between two  $\text{TiO}_2\text{-B}$  grains, and these clearly have an epitaxial relationship with the neighboring  $\text{TiO}_2\text{-B}$  grains, as shown in Fig. 9c. These are not stand-alone grains formed directly from the STO substrate but possibly formed as high temperature derivatives of bronze-type grains under topotactic reaction as has been reported in the literature,<sup>32</sup> judging from their atomic configuration. The formation of  $\text{TiO}_2\text{-A}$  grains most likely occurred via shearing of the two (-201)  $\text{TiO}_2\text{-B}$  planes along the [102] direction by  $0.42c$ . After the reaction, (103) planes of a newly formed  $\text{TiO}_2\text{-A}$  grain is under epitaxy with  $\text{TiO}_2\text{-B}$  planes, forming a periodic boundary as shown in Fig. 9d.

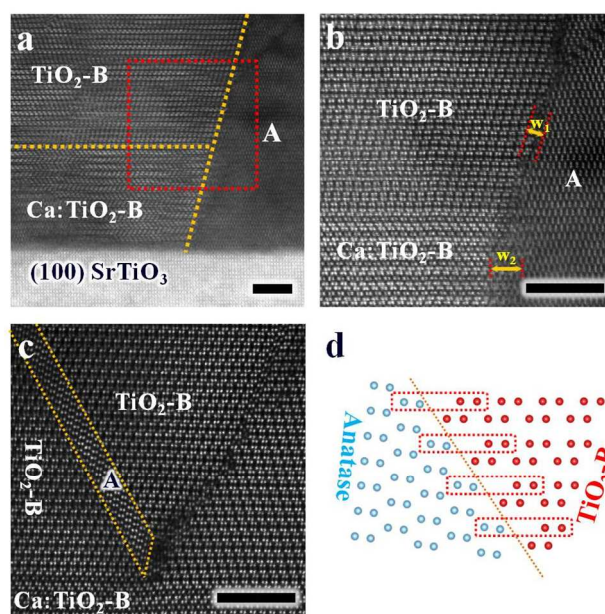


**Fig. 9** High-resolution STEM Images of (a,b) an interphase boundary between an anatase grain grown directly on (100) STO substrate independent from  $\text{TiO}_2\text{-B}$  and  $\text{Ca}:\text{TiO}_2\text{-B}$  and (c) an anatase micro-grain epitaxially formed between the two  $\text{TiO}_2\text{-B}$  grains along with a (d) schematics of bonding between periodic boundary formed between anatase and  $\text{TiO}_2\text{-B}$  grains. Scale bars are 5nm.

#### 4. Conclusions

In summary, thin films of monoclinic  $\text{TiO}_2\text{-B}$  and  $\text{Ca}:\text{TiO}_2\text{-B}$  were grown on (100) and (110) cubic STO substrates in order to study the effect of substrate orientation on film morphology and the nature of defects present in the films. By employing aberration-corrected STEM, we have analyzed both interfacial structure at phase boundaries and identified a variety of

interesting defect structures. Although the growth of a Ca:TiO<sub>2</sub>-B film on the (100) substrate is highly c-oriented, the growth on the (110) substrate is affected by phase separation induced formation of the secondary phase, cubic CaTiO<sub>3</sub> that acts as a heterogeneous self-template for the crystallographically tilted growth of TiO<sub>2</sub>-B grains. For c-axis Ca:TiO<sub>2</sub>-B growth on a (100) substrate, SSTs at the STO surface induce local atomic ordering near the interface between Ca:TiO<sub>2</sub>-B and STO. However, for growth on a (110) substrate, a-direction growth of a TiO<sub>2</sub>-B layer separated from CTO induces only several planar stacking defects associated with a Ca-modified TiO<sub>x</sub> layer but does not affect Ca:TiO<sub>2</sub>-B deposited along the c-axis. For c-axis TiO<sub>2</sub>-B film growth on a (001) Ca:TiO<sub>2</sub>-B template, out-of-phase boundaries are nucleated out of the plane with a missing Ca-modified TiO<sub>x</sub> layer. This understanding of film growth mechanism and defect formation should provide an important step toward successful fabrication of high-performance energy devices.

### Acknowledgements

This work was supported by the Center for Solar and Thermal Energy Conversion, an Energy Frontier Research Center funded by the U.S. Department of Energy, Office of Science, Office of Basic Energy Sciences, under Award Number DE-SC0000957. Also, this work was partially supported by Ford Motor Company, under a University Research Proposal grant, and the National Science Foundation, through Grant CBET-1159240.

### Notes and references

<sup>a</sup>Department of Materials Science and Engineering, University of Michigan, 2300 Hayward Street, Ann Arbor, MI 48109, USA

<sup>b</sup>Department of Chemical Engineering and Materials Science and Department of Physics and Astronomy, University of California - Irvine, 816 F Engineering Tower, Irvine, CA 92697, USA

†Electronic Supplementary Information (ESI) available: Figs. s1-s5 See DOI: 10.1039/b000000x/

- 1 S.-W. Cheong, *Nat. Mater.*, 2007, **6**, 927-928.
- 2 I. Grinberg, D. V. West, M. Torres, G. Gou, D. M. Stein, L. Wu, G. Chen, E. M. Gallo, A. R. Akbashev, P. K. Davies, J. E. Spanier and A. M. Rappe, *Nature*, 2013, **503**, 509-512.
- 3 P. Poizot, S. Laruelle, S. Grugeon, L. Dupont and J. M. Tarascon, *Nature*, 2000, **407**, 496-499.
- 4 A. G. Dylla, G. Henkelman and K. J. Stevenson, *Acc. Chem. Res.*, 2013, **46**, 1104-1112.
- 5 A. R. Armstrong, G. Armstrong, J. Canales, R. Garcia and P. G. Bruce, *Adv. Mater.*, 2005, **17**, 862-865.
- 6 R. Marchand, L. Brohan and M. Tournoux, *Mater. Res. Bull.*, 1980, **15**, 1129-1133.
- 7 M. Ben Yahia, F. Lemoigno, T. Beuvier, J.-S. Filhol, M. Richard-Plouet, L. Brohan and M.-L. Doublet, *J. Chem. Phys.*, 2009, **130**, 204501.
- 8 A. Vittadini, M. Casarin and A. Selloni, *J. Phys. Chem. C*, 2009, **113**, 18973-18977.

- 9 W. Liu, J.-g. Wang, W. Li, X. Guo, L. Lu, X. Lu, X. Feng, C. Liu and Z. Yang, *Phys. Chem. Phys. Chem.*, 2010, **12**, 8721-8727.
- 10 C. Arrouvel, S. C. Parker and M. S. Islam, *Chem. Mater.*, 2009, **21**, 4778-4783.
- 11 M.-C. Yang, Y.-Y. Lee, B. Xu, K. Powers and Y. S. Meng, *J. Power Sources*, 2012, **207**, 166-172.
- 12 H. Liu, Z. Bi, X.-G. Sun, R. R. Unocic, M. P. Paranthaman, S. Dai and G. M. Brown, *Adv. Mater.*, 2011, **23**, 3450-3454.
- 13 K. Zhang, M. B. Katz, B. Li, S. J. Kim, X. Du, X. Hao, J. R. Jokisaari, S. Zhang, G. W. Graham, A. Van der Ven, B. M. Bartlett and X. Pan, *Adv. Mater.*, 2014, **26**, 7365-7370.
- 14 C.-C. Tsai, Y.-Y. Chu and H. Teng, *Thin Solid Films*, 2010, **519**, 662-665.
- 15 J. Procházka, L. Kavan, M. Zukulová, O. Frank, M. Kalbáč, A. Zukal, M. Klementová, D. Carbone and M. Graetzel, *Chem. Mater.*, 2009, **21**, 1457-1464.
- 16 L. Fernández-Werner, R. Faccio, A. Juan, H. Pardo, B. Montenegro and Á. W. Mombrú, *Appl. Surf. Sci.*, 2014, **290**, 180-187.
- 17 L. Qi, Y. Liu and C. Li, *Appl. Surf. Sci.*, 2010, **257**, 1660-1665.
- 18 B. Wang, H. Xin, X. Li, J. Cheng, G. Yang and F. Nie, *Sci. Rep.*, 2014, **4**, 1-7.
- 19 A. R. Armstrong, G. Armstrong, J. Canales and P. G. Bruce, *J. Power Sources*, 2005, **146**, 501-506.
- 20 V. Augustyn, P. Simon and B. Dunn, *Energy Environ. Sci.*, 2014, **7**, 1597-1614.
- 21 T. Hamada, A. Ito, E. Fujii, D. Chu, K. Kato and Y. Masuda, *J. Cryst. Growth*, 2009, **311**, 3687-3691.
- 22 W. Guo, M. B. Katz, C. T. Nelson, T. Heeg, D. G. Schlom, B. Liu, Y. Che and X. Q. Pan, *Appl. Phys. Lett.*, 2009, **94**, 122107.
- 23 K. Zhang, X. Du, M. B. Katz, B. Li, S. J. Kim, K. Song, G. W. Graham and X. Pan, *Chem. Commun.*, 2015, *Accepted*.
- 24 C. K. Ong and S. J. Wang, *Appl. Surf. Sci.*, 2001, **185**, 47-51.
- 25 C. Ma, M. Liu, C. Chen, Y. Lin, Y. Li, J. S. Horwitz, J. Jiang, E. I. Meletis and Q. Zhang, *Sci. Rep.*, 2013, **3**, 1-5.
- 26 C. R. Connell, R. E. Caflisch, E. Luo and G. Simms, *J. Comput. Appl. Math.*, 2006, **196**, 368-386.
- 27 R. Takahashi, H. Misumi and M. Lippmaa, *Cryst. Growth Des.*, 2012, **12**, 2679-2683.
- 28 K. Zhang, S. J. Kim, Y. Zhang, T. Heeg, D. G. Schlom, W. Shen and X. Pan, *J. Phys. D: Appl. Phys.*, 2014, **47**, 105302.
- 29 M. A. Zurbuchen, W. Tian, X. Q. Pan, D. Fong, S. K. Streiffner, M. E. Hawley, J. Lettieri, Y. Jia, G. Asayama, S. J. Fulk, D. J. Comstock, S. Knapp, A. H. Carim and D. G. Schlom, *J. Mater. Res.*, 2007, **22**, 1439-1471.
- 30 I. MacLaren, L. Wang, O. Morris, A. J. Craven, R. L. Stamps, B. Schaffer, Q. M. Ramasse, S. Miao, K. Kalantari, I. Sterianou and I. M. Reaney, *APL Mat.*, 2013, **1**, 021102.
- 31 L. Q. Wang, B. Schaffer, I. MacLaren, S. Miao, A. J. Craven and I. M. Reaney, *J. Phys.: Conf. Ser.*, 2012, **371**, 012036.
- 32 L. Brohan, A. Verbaere, M. Tournoux and G. Demazeau, *Mater. Res. Bull.*, 1982, **17**, 355-361.

## Table of contents entry

An atomic-scale analysis of interfacial structure and defects in  $\text{CaTi}_5\text{O}_{11}$  grown on  $\text{SrTiO}_3$  and  $\text{TiO}_2\text{-B}$  grown on  $\text{CaTi}_5\text{O}_{11}$  is presented.

